

Large-Eddy Simulation of Pressure Transport Below the Mixed Layer

Roland W. Garwood, Jr. and Ramsey R. Harcourt

Naval Postgraduate School, Monterey, California 93943

Abstract. Deep convection energizes the entire water column. Large-eddy simulation of the oceanic boundary layer system predicts turbulence in the well-mixed layer as well as turbulence-induced internal waves propagating into the underlying stratified water column of the freely convecting wintertime Labrador Sea. Of particular interest is the downward propagation of energy from the turbulent boundary layer by pressure transport and the buildup of internal wave energy in response to local atmospheric forcing. A near equilibrium internal wave spectrum is approached after about two weeks of episodic storm cooling. A broad band omnidirectional internal wave field with peak energy near the buoyancy frequency N is forced mostly by the surface buoyancy flux. The pressure transport of mixed-layer kinetic energy carries about 30 % of the available energy into the stratified zone and causing entrainment. On average, 10^{-4} W/m² or about 1% of the winter Labrador Sea mixed-layer energy escapes into the pycnocline where it is converted into internal wave energy.

1. Introduction

There is much interest in describing the internal wave field and understanding the sources and sinks for this energy in the ocean interior. The capability to predict the variety of phenomena responsible for internal wave generation, propagation and ultimate dissipation and mixing is necessary to understand and predict the distribution of mass, energy and momentum in the ocean interior. At the 1991 Hawaiian Winter Workshop many investigators reported on the broad aspects of the problem, and the meeting proceedings (*Muller and Henderson, 1991*) and subsequent journal articles provide valuable references and an understanding of the complex nature of these non-linear problems.

Here we focus only on a single source and pathway of internal wave energy by asking the question, "How much locally generated kinetic energy escapes the mixed layer to generate internal waves and ultimately to cause mixing and dissipation in the underlying pycnocline?" To answer this question for a specific well-observed case, the dynamical system response of the Labrador Sea water column to realistic surface forcing has been simulated numerically using oceanic large-eddy simulation (*Garwood et al., 1994; Harcourt et al., 1998; Harcourt, 1999*). The Labrador Sea deep convection field experiment, 1996-1998, is yielding a wealth of observations to initialize, force, and ultimately to verify model results (*The Lab Sea Group, 1999*).

2. Numerical Experiment

To focus on the problem here, Figure 1 is presented to define the problem and illustrate the nature of the results. This figure depicts the model-predicted internal wave field generated by the turbulence in the surface mixed layer. At the instant of this picture on Julian day 63 of

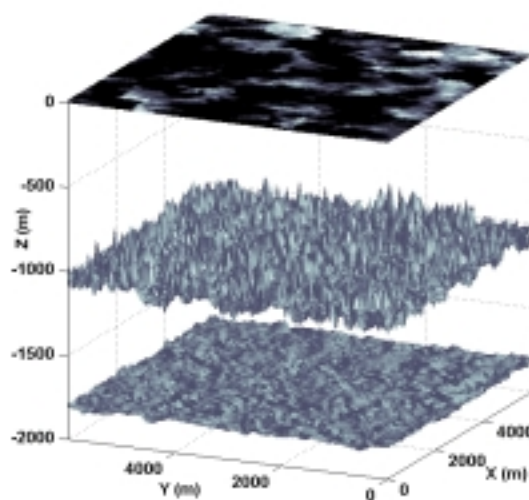


Figure 1. Sea surface temperature showing the surface manifestation of Rayleigh-Benard convection cells above isopycnic surfaces vertically distorted by internal waves in the Labrador Sea pycnocline.

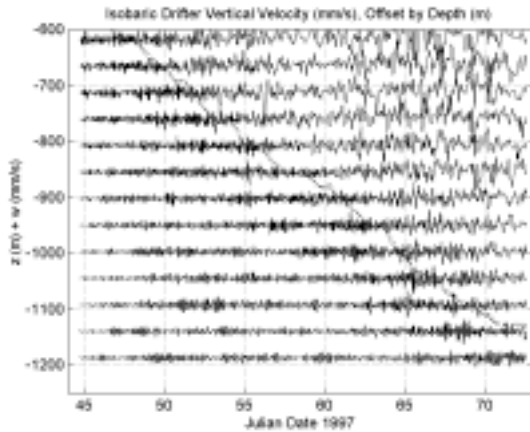


Figure 2. LES-predicted vertical velocity for isobaric drifters (solid) and mixed layer depth (dotted) for winter 1997 in Labrador Sea, from *Harcourt* (1999).

1997, the numerical model had simulated about 20 days of ocean response to synoptic atmospheric forcing. In the picture, the vertical displacements by the internal waves exceed 30 m on the km-deep density iso-surface just beneath the mixed layer. Wave displacements are on the order of 5 m on the iso-surface near $z = -2$ km. A well-mixed layer is at the top of this coupled turbulence-internal gravity wave system. The mixed layer coincides approximately with the fully turbulent boundary layer. It extends from the ocean surface at $z = 0$ downward to the beginning of the nonturbulent pycnocline at $z = -h$. In the course of 28 days during winter 1997 at 57N, 54W in the Labrador Sea, h deepened from less than 600 m to more than 1100 (Figure 2). The vertical velocities shown in this figure were “observed” by simulating freely drifting isobaric floats distributed randomly in the LES domain. Data collected by these floats augment considerably the sampling in time of both the turbulence and the internal waves. The fluctuating vertical velocity and buoyancy above $z = -h$ in Figure 2 are associated with turbulence; below $z = -h$ the vertical velocity and displacement are attributable to internal waves. Figure 3 is a representative N^2 profile. At the time of this profile, Julian day 63, the maximum stratification of $N=10^{-3}\text{s}^{-1}$ is at the base of the mixed layer near $z = -950$ m.

Between $z = 0$ and $z = -h$, turbulent kinetic energy (TKE) is produced by shear production (forced convection) and upward buoyancy flux (free convection). This TKE is mostly dissipated or converted to potential energy by downward buoyancy flux in the entrainment zone immediately beneath the well-mixed layer. For the Labrador Sea profile on day 63, the entrainment zone is the region of sharply increased N , which is about 200 m thick. The downward buoyancy flux in this zone is associated with entrainment or “penetrative convection.” Typically, up to

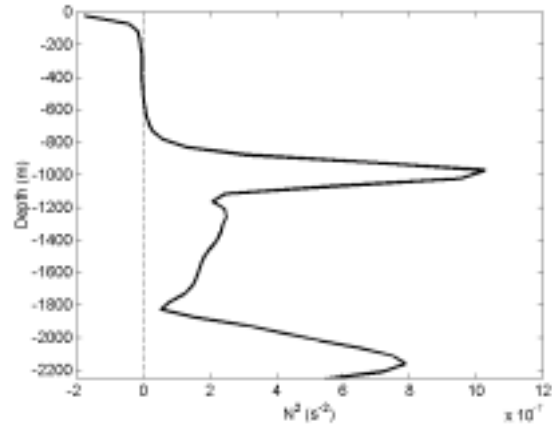


Figure 3. N^2 profile for 1 March 1997.

about 20-30% of the total mixed layer TKE may be converted into potential energy by penetrative convection. But how much energy escapes below the entrainment zone? The purpose of this paper is to answer this question using a nonhydrostatic model for the complete mixed layer-pycnocline system that includes actually observed surface forcing and the most complete model physics available to predict unsteady three-dimensional realization of both turbulence and internal waves.

2.1. Why is Large-Eddy Simulation Needed Here, and What are the Model Requirements?

Large-eddy simulation (LES) is necessary and appropriate for this problem because the same model that was originally developed for robust prediction of geophysical turbulence can predict the nonlinear forcing by wave-wave interactions in the pycnocline. Originally developed to predict three-dimensional unsteady turbulence in the atmosphere (*Deardorff*, 1973; *Moeng*, 1984), LES was extended to oceanic application in the polar seas by *Garwood et al.* (1994). Others including *Skylingstad and Denbo* (1995) have subsequently conducted nonhydrostatic large-eddy simulation of deep ocean convection, but none of these examine the internal wave field generated by the mixed layer turbulence. Conversely, *Siegel and Domaradski* (1994) simulated internal waves in decaying stratified turbulence, isolated from the original surface forcing.

More recently, oceanic applications (*Harcourt et al.*, 1998; *Harcourt*, 1999) have embedded drifter models of a variety of designs (e.g., *Rosby et al.*, 1986; *Davis et al.*, 1992; *D'Asaro*, 1996) into the LES domain. *Lherminier et al.* (1999) have used these LES drifter predictions to help understand actual drifter observations in the Greenland Sea. Some of these hypothetical drifter results are useful here for understanding internal waves. Another recent

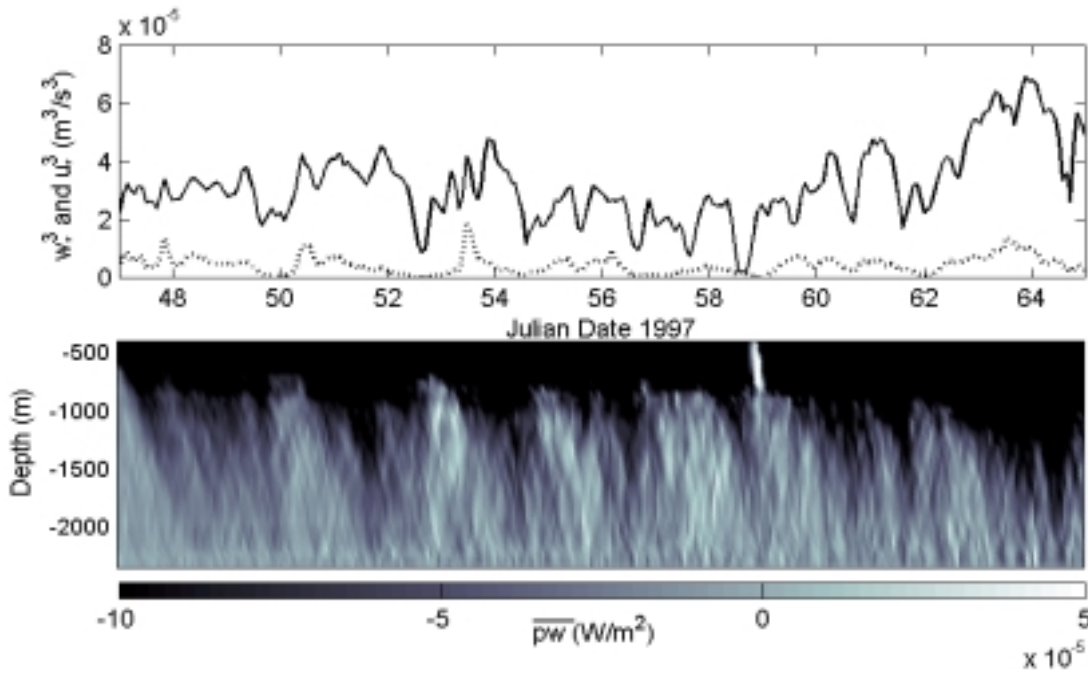


Figure 4. (Upper) Surface forcing: w_*^3 (solid) and u_*^3 (dotted). (Lower) Pressure transport simulated in pycnocline beneath mixed layer during February and March 1997 in the Labrador Sea.

oceanic LES study involves the interaction between surface-forced convection and larger-scale oceanic flows (Stone, 1999), and this may be a precursor of larger-scale

LES investigation of internal wave propagation. Collectively these several references provide more detailed explanations of LES, and computational issues are not emphasized. However, some important LES issues are listed here.

With regard to realistic prediction of the ocean mixed layer, LES needs to include the physical processes of the mixed-layer eddies that contain most of the energy and buoyancy variance of the turbulence. These “large eddies” are responsible for the buoyancy flux and Reynolds stresses. To accomplish this, an LES model must resolve scales from the largest turbulence motion (integral scale) down to and including the upper portion of the inertial subrange of the turbulence, exhibiting the expected $K^{-5/3}$ cascade of energy.

As a practical matter, if the turbulence integral length scale is approximated by h , LES for oceanic free convection is able to accomplish this first objective well with a grid size $\Delta x = \Delta y = \Delta z = h/25$ or smaller. Also required is a proven combination of filtering and application of a realistic TKE budget-based subgrid eddy viscosity/conductivity/diffusivity, $K_{M/T/S}$, in the momentum, potential temperature, and salinity budgets. Then $K_{M/T/S}$ values are kept to a minimum. This “mops up” the high wavenumber variances created by aliasing and the energy cascade, without unduly damping the flux-supporting and energy-containing integral scale eddies. Then the effective model Reynolds number can be sufficiently large ($Re_M = w_*h/K_M > 2000$) to establish a geophysically real-

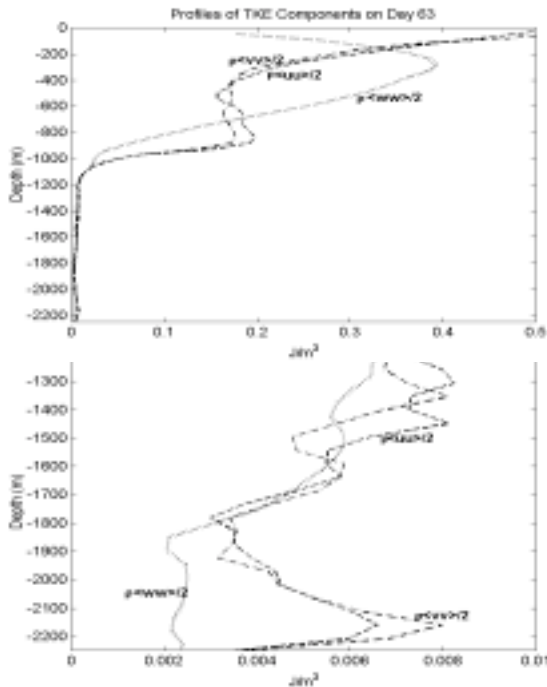


Figure 5. Horizontally averaged TKE profiles on day 63 of 1997 for (a) entire water column, and (b) below mixed layer with expanded scale.

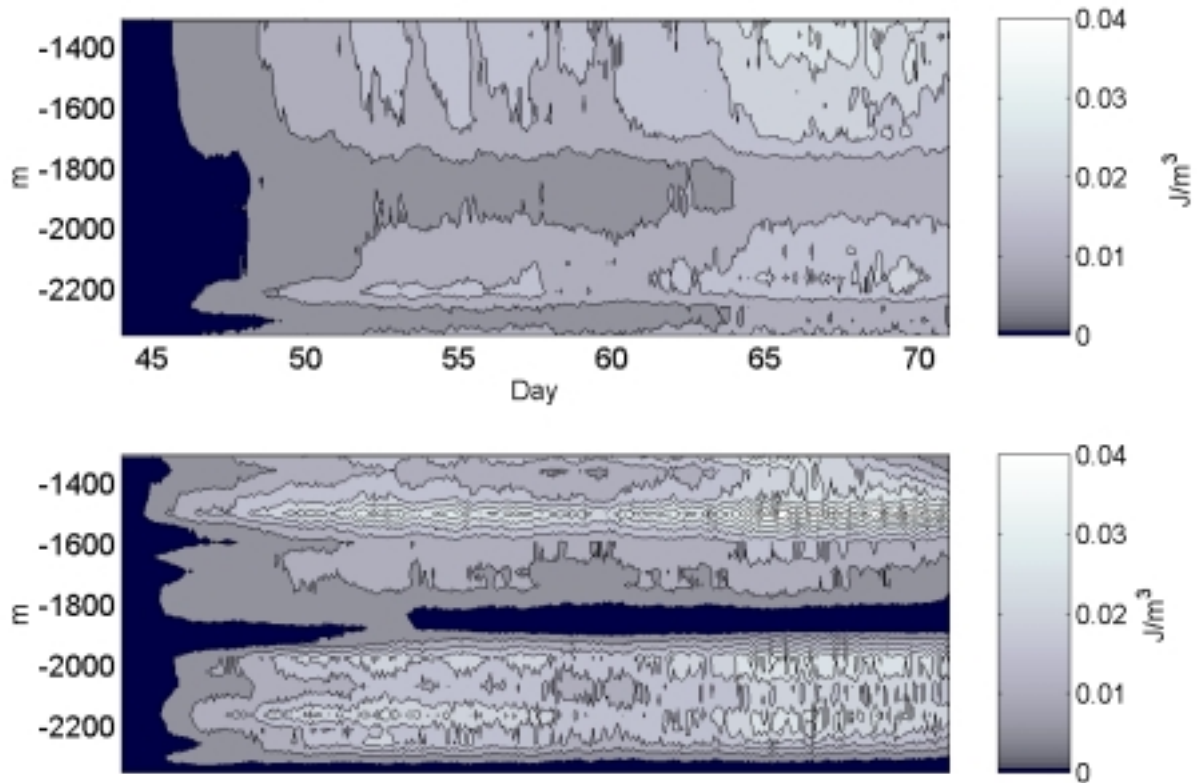


Figure 6. (a) Vertical kinetic energy and (b) wave potential energy versus time and depth in the pycnocline well beneath the surface mixed layer.

istic inertial subrange. Here w_* is the free convection velocity scale that depends upon mixed layer depth and the surface buoyancy flux B_0 . Low-pass filtering during the course of model integration is necessary to reduce aliasing at the highest wavenumbers and to prevent numerical instability.

The horizontal and vertical grid sizes should be equal in order to resolve well the approximately isotropic inertial subrange. Furthermore, to minimize any artificial resonance or a box mode, the scale size L_H of the model horizontal domain needs to be bigger than several integral scales, or $L_H > 5h$. These requirements are satisfied here, with h increasing during the course of the numerical solution from about 600 m to 1000 m, by employing a grid size between 25 m and 50 m with $128 \times 128 \times 50$ grid points in the two horizontal and vertical coordinates, respectively. The model time step Δt is constrained by the c-f-l condition to be less than the resolved length scale divided by the largest resolved convective velocity. For the widely fluctuating intensity of convection during the winter Labrador Sea numerical experiments, a Δt of 2 minutes meets this requirement.

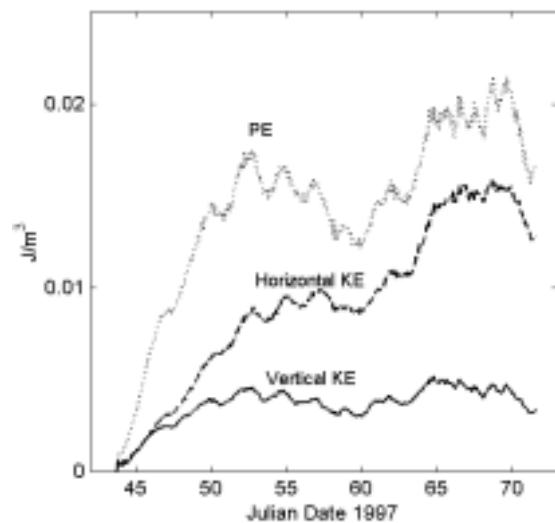


Figure 7. Vertically integrated wave kinetic energy and potential energy, from $z = -2300$ m to $z = -1200$ m.

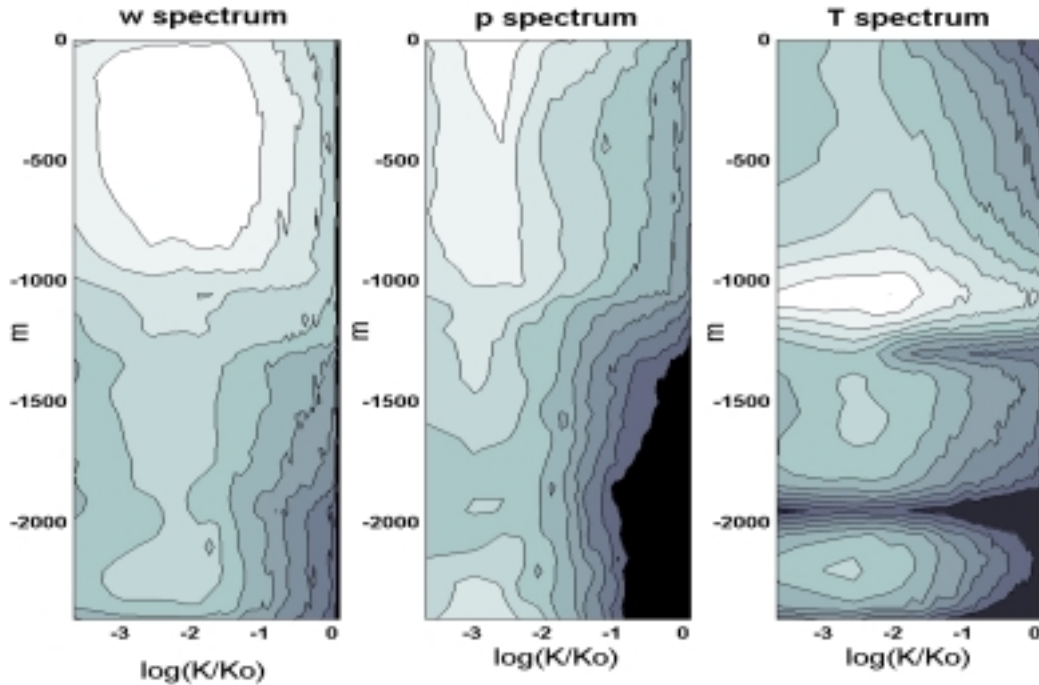


Figure 8. Wavenumber spectra versus depth for 28-day period during winter 1997 in Labrador Sea.

With regard to realistic prediction of internal waves in the pycnocline, *Siegel and Domaradski* (1994) delineate LES requirements. In short, LES for mixed layer-generated internal waves includes the same nonhydrostatic physics that maintains mixed-layer turbulence. A possible difference in internal wave prediction is that Δt needs to resolve the largest buoyancy frequency N_{\max} , or $\Delta t \ll N_{\max}^{-1}$. For the N^2 profile shown in Figure 3, the N_{\max} is 10^{-3}s^{-1} . Hence the 2-min value of Δt is more than adequate for both mixed layer turbulence and the highest-frequency internal waves of consequence possible at this location in the Labrador Sea.

2.2. Surface Forcing

Surface forcing was provided by time series of the wind stress $\tau(t)$ and the surface buoyancy flux, $B_o(t)$. The period of the numerical experiment coincided with the period of observed forcing in the Labrador Sea experiment during February and March 1997. These time series were calculated *in situ* from the R/V *Knorr*, as documented by *The Lab Sea Group* (1999). For the purposes of this study of the energy budgets and propagation of energy into the interior, the surface forcing in Figure 4 is presented in terms of kinematic energy per unit area, or the cube of the forcing velocity scales u_* and w_* . The forced convection velocity scale is $u_* = (\tau/\rho)^{1/2}$, and the free convection velocity scale is $w_* = (B_o h/2)^{1/3}$.

As Figure 4 shows, the free convection forcing is usually several times larger than the forced convection. The largest free convection forcing of $w_*^3 = 6.8 \times 10^{-5} \text{ m}^3/\text{s}^3$ occurred on day 64. This largest forcing was associated with a net upward surface heat loss to the atmosphere and the sky of nearly $700 \text{ W}/\text{m}^2$. This heat flux causes a surface buoyancy flux of $B_o = 1.43 \times 10^{-7} \text{ m}^2/\text{s}^3$, and the mixed layer depth was $h = 949 \text{ m}$ at the time. The time-averaged free convective forcing for the entire numerical experiment was $\langle w_*^3 \rangle = 3.01 \times 10^{-5} \text{ m}^3/\text{s}^3$. The time-average of the forced convection forcing was $\langle u_*^3 \rangle = 0.35 \times 10^{-5} \text{ m}^3/\text{s}^3$, nearly an order of magnitude smaller than the forcing by the buoyancy flux. Both u_* and w_* vary in time with the periodic synoptic storm forcing, and this is important for the transient nature of the mixed layer turbulence and the propagation of energy into the interior by pressure transport, or pressure-velocity correlation, $\langle pw \rangle$. The lower panel of Figure 4 shows $\langle pw \rangle(t, z < -h)$, which was calculated from the LES-predicted fields. The downward pressure transport below the mixed layer is obviously synchronized with the surface forcing.

3. Turbulent and Wave Energy, Budgets and Fluxes

3.1. Turbulent and Wave Kinetic Energy

The fluctuating kinetic energy may be partitioned between turbulent kinetic energy (TKE) and internal wave kinetic energy (IWKE). Figure 5 shows the total turbulent plus internal wave kinetic energy at an instant during day 63. There is a maximum vertical KE at about -300 m and a shoulder just below -1000 m. The maximum energy is entirely TKE. The shoulder is attributable to IWKE and is coincident with the large stratification just beneath the mixed layer. The snapshot in Figure 1 of the internal wave field showed the largest internal waves with amplitudes exceeding 30 m just below the mixed layer. The internal waves in the underlying pycnocline have a root-mean-square amplitude of about 10 m. The peak vertical velocity observed by the isobaric drifters situated in the steep pycnocline just beneath the mixed layer in Figure 2 is about 10 mm/s. This is consistent with a vertical kinetic energy of about 0.02 J/m³ in the vicinity of $z = -1050$ m in Figure 5.

Figure 6 shows that the wave kinetic and potential energy fields vary considerably in response to the episodic surface forcing. The time series of the vertical averages for wave potential and kinetic energy (Figure 7) show the effect of this episodic forcing. The wave energy has a net growth trend for the 28-day period; however, the wave energy spins up most rapidly during the first couple weeks of the numerical solution.

Variability in internal wave energies in the vertical is linked to stability. As a rule here, the largest values of wave energy are associated with the pycnocline immediately beneath the mixed layer. In both Figures 5 and 6, secondary maxima in wave energies near $z = -2100$ m are associated with a second peak in stability. This second stable zone is remnant from the mixed layer that deepened to about 2000 m during the previous winter, and it is evident in the N^2 profile in Figure 3.

As suggested by Figures 6 and 7, the internal wave field takes about a week to spin up to an approximate equilibrium. Horizontal wavenumber spectra for the vertical velocity, pressure and temperature were calculated from this point in time, day 50, until the end of the numerical experiment. Figure 8 shows the depth dependence of the horizontal wavenumber spectra. Within the mixed layer, spectra of vertical velocity, potential temperature and salinity (not shown) all have a $K^{-5/3}$ inertial subrange that span a decade of increasing wave number. The peak energy and variances in the mixed layer correspond closely to the wavenumber $K_0 = 1/h$, indicating the strong influence of vertical convection on the horizontal scale of the Rayleigh-Benard convection cells (Carsey and Gar-

wood, 1993). The peak variances at 1100 m and 2100 m depths are especially obvious in the temperature spectra.

Below the mixed layer, the horizontal wavenumber fall off to approximately K^{-1} (Figures 8 and 9a). From the time series of vertical velocity sensed by a simulated drifter beneath the large gradient region, near $z = -1200$ m, a frequency spectrum was also calculated (Figure 9b). The frequency spectrum peaks at the buoyancy frequency N for this depth, and it resembles the frequency spectrum of the freely convective atmosphere (Fritts *et al.*, 1990).

3.2 Turbulent and Wave Kinetic Energy Budgets and Fluxes

The dissipation ε and the buoyancy flux $\langle bw \rangle$ dominate the TKE budget in most of the freely convecting mixed layer during day 63 (Figure 10a), except near the surface and the entrainment zone. In the upper 100 m, the shear production is the dominant source of turbulence. In the entrainment zone between $z = -780$ m and -1000 m, the buoyancy flux is negative because of entrainment of

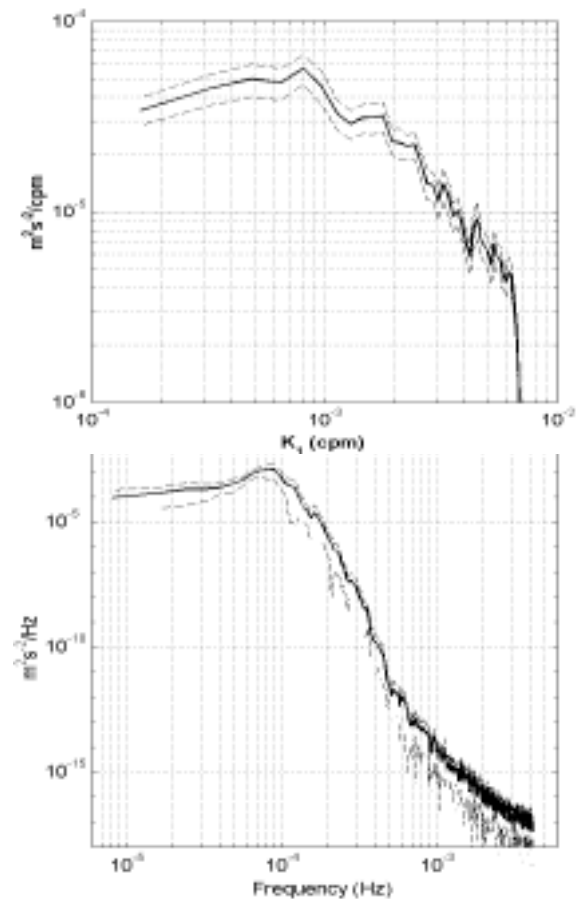


Figure 9. (a) Horizontal wavenumber and (b) frequency spectra at 1200-m depth

dense fluid from below into the mixed layer. In this region there is an approximate balance between the buoyant damping by entrainment and the convergence of pressure and turbulent transport.

Below the mixed layer, the approximate balance between buoyancy flux and the convergence of transport is continued (Figure 10b). An important difference from the entrainment zone, however, is that the buoyancy flux below the mixed layer goes to increase the wave potential energy; in the entrainment zone, the buoyancy flux increases the mean potential energy by mixing. Another important difference is that the transport of energy below the mixed layer is accomplished almost entirely by the pressure transport, $\langle pw \rangle$, while turbulent transport is large only in the overlying turbulent boundary layer (Figure 11a).

Figure 11b plots the pressure transport below the mixed layer, averaged for the entire period of the simulation. The mean downward energy flux is 0.1 mW/m^2 at z

$= -1100 \text{ m}$ and is reduced to half this value by $z = -1300 \text{ m}$. Included in Figure 11b is the pressure transport for an instant during day 63. The pulse-like form is caused by the episodic nature of the surface forcing. The slanted structure in the $\langle pw \rangle(t, z)$ field (Figure 4) is attributable to this phase lag, and its slope corresponds to a downward propagation of energy-transporting events at a speed of approximately 1 km/day . Figures 4 and 11b together demonstrate the importance of episodic storms, causing order of magnitude temporal and spatial fluctuations in the energy flux downward.

4. Conclusions

Verification of these model results is yet to be accomplished but will be done by comparison with the Labrador Sea drifters deployed during 1997 and 1998 (designs of Rossby *et al.*, 1986; Davis *et al.*, 1992; D'Asaro, 1996). However, some conclusions may be readily drawn. In

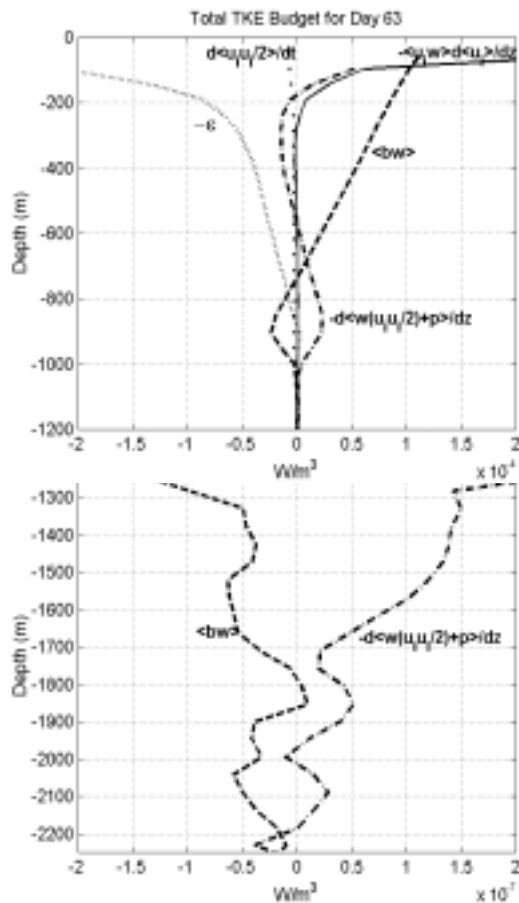


Figure 10. Average TKE budget for 28-day period for (a) upper 1200 m of water column, and (b) below mixed layer with expanded scale.

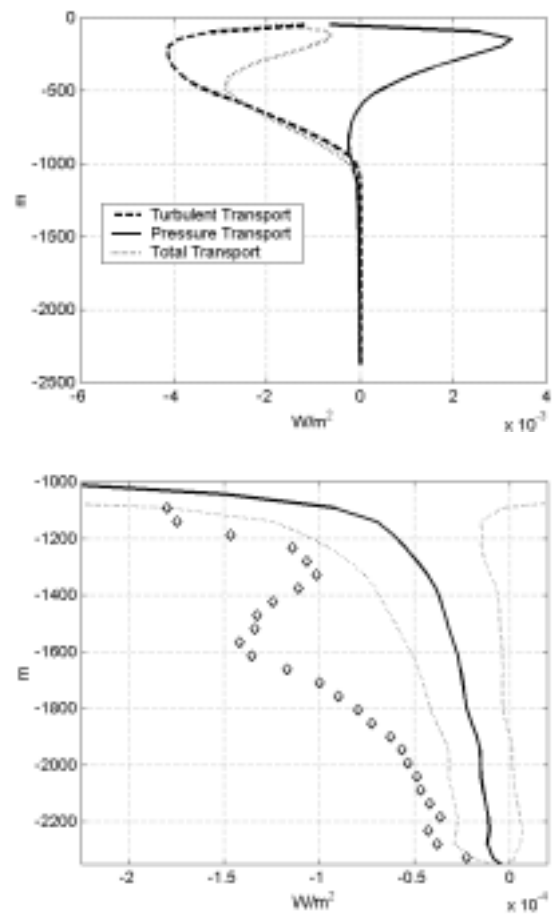


Figure 11. Vertical transport of energy averaged for 28-days for (a) entire water column. (b) Pressure transport below mixed layer with expanded scale. Diamonds are pressure transport during day 63, and dotted curves are plus and minus one standard deviation.

modeling the mixed layer, the system has often been approximated as closed, without energy escaping below the entrainment zone. Hence, to predict entrainment, a closed-system TKE budget is invoked that balances entrainment damping with net production minus dissipation. In such a system, transport redistributes TKE within the mixed layer and increases mixed layer potential energy by penetrative convection; however, energy that escapes below the entrainment zone into the pycnocline has been neglected.

The energy that escapes the mixed layer and the entrainment zone may be small compared with the total TKE. However, the escaped energy may be significant for the ambient internal wave energy in the pycnocline. The issue in this paper concerned the propagation or transport of TKE below the entrainment zone, energizing the internal wave field and possibly causing dissipation and mixing in the pycnocline. For the Labrador Sea site, the deep stratified water column from -1000 m to -2300 m was examined, and the loss of energy into the interior averaged about 0.1 W/m^2 . This energy loss of less than 1% of the mixed layer and the entrainment zone energy is usually insignificant for mixed layer dynamics and the prediction of mixed layer depth and surface conditions including sea surface temperature. However, this is not a negligible energy flux with regard to the maintenance of the interior internal wave field when other sources of internal wave energy are minimal.

LES was demonstrated to be an effective tool to quantify the generation and vertical propagation of internal wave energy by local forcing. To include nonlocal sources of internal wave energy, including bottom boundary layer and inertial-gravity wave sources, a much larger horizontal model domain will be required. To still include the interaction between the internal waves and the turbulence, the grid resolution will have to be relatively high. The computing resources are sufficient today to tackle this problem in depth-limited domains, such as on the continental shelf. To further complete the problem, the roles of forced convection in shallow stable mixed layers and of surface gravity waves needs to be added (Watson, 1990) to this study which focused only on deep free convection.

Acknowledgments. The Office of Naval Research (Code 322OM) and the National Science Foundation (Award Number 9530530) sponsored this work, and the DOD HPC Center provided a grant of computing time. This support is gratefully acknowledged. We thank Peter Guest for providing the surface fluxes soon after completion of the winter 1997 field experiment, and we thank John Lazier for the hydrographic data to initialize the model. Discussions with Pascale Lherminier were very helpful.

References

- Carsey, F. D. and R. W. Garwood, Jr., Identification of modeled ocean plumes in Greenland Gyre ERS-1 SAR data, *Geophys. Res. Lett.*, 20, 2207-2210, 1993.
- D'Asaro, E. A., A Lagrangian float, *J. Atmos. Oceanic Technol.*, 13, 1230-1246, 1996.
- Davis, R. E., D. C. Webb, L. A. Regier, and J. Dufour, The autonomous Lagrangian circulation explorer (ALACE), *J. Atmos. Oceanic Technol.*, 9, 264-285, 1992.
- Deardorff, J. W., The use of subgrid transport equations in a three-dimensional model of atmospheric turbulence, *J. Fluids Engineering*, 429-438, 1973.
- Fritts, D. C., U.-P. Hoppe, and B. Inhester, A Study of the vertical motion field near the high-latitude summer menopause during MAC/SINE, *J. Atmos. Terres. Phys.*, 52, 927-938, 1990.
- Garwood, R. W., Jr., S. M. Isakari and P. C. Gallacher, Thermobaric convection, in *The Role of the Polar Oceans in Shaping the Global Environment*, Ed. by O. Johannessen, R. Muench and J. Overland, Am. Geophys. Union Monograph, Vol. 85, 199-209.
- Harcourt, R. R., Numerical simulation of deep convection and the response of drifters in the Labrador Sea, Ph. D. Dissertation, Univ. of California, Santa Cruz, 378 pp., 1999.
- Harcourt, R. R., L. Jiang, and R. W. Garwood, Jr., Numerical simulation of drifter response to Labrador Sea convection, Tech. Rep. NPS-OC-98-001, Naval Postgraduate School, Monterey, 71 pp., 1998.
- Lherminier, P., R. R. Harcourt, R. W. Garwood, Jr., and J.-C. Gascard, Interpretation of mean vertical velocities measured by isobaric floats during deep convective events, *J. Mar. Systems*, submitted, 1999.
- Moeng, C.-H., A large-eddy simulation model for the study of boundary-layer turbulence, *J. Atmos. Sci.*, 41, 2052-2062, 1984.
- Müller, P. and D. Henderson, Eds., *Dynamics of Oceanic Internal Gravity Waves, Proceedings 'Aha Huliko'a Hawaiian Winter Workshop*, University of Hawaii at Manoa, 15-18 January, 508 pp., 1991.
- Rosby, T., D. Dorson, and J. Fontaine, The RAFOS system, *J. Atmos. Oceanic Technol.*, 3, 672-679, 1986.
- Siegel, D. A. and J. A. Domaradzki, Large-eddy simulation of decaying stably stratified turbulence, *J. Phys. Oceanogr.*, 24, 2353-2386, 1994.
- Skyllingstad, E. D. and D. W. Denbo, An ocean large-eddy simulation of Langmuir circulation and convection in the surface mixed layer, *J. Geophys. Res.*, 100, 8501-8522, 1995.
- Stone, R. E., Entrainment, detrainment and large-scale horizontal gradients in oceanic deep convection, Ph.D. thesis, Naval Postgraduate School, Monterey, 123 pp., 1999.
- The Labrador Sea Group, The Labrador Sea deep convection experiment, *Bull. Am. Meteorol. Soc.*, 79, 2033-2058, 1998.
- Watson, K. M., The coupling of surface and internal gravity waves: Revisited, *J. Phys. Oceanogr.*, 20, 1233-1248, 1990.